Supplementary information for

Kinetic modeling of stem cell transcriptome dynamics to identify regulatory modules of normal and disturbed neuroectodermal differentiation

Johannes Meisig, Nadine Dreser*, Marion Kapitza, Margit Henry, Tamara Rotshteyn, Jörg Rahnenführer, Jan G. Hengstler, Agapios Sachinidis, Tanja Waldmann, Marcel Leist# and Nils Blüthgen#*

**,# shared first/ last author*

Table of contents

Supplementary Figures

S1 **Primary antibodies used for the study**

S2 **Primer background information**

S3 **Wnt signaling and its consequences in the STOP-tox$_{(UKN)}$ assay**

S4 **Attenuation of neural crest differentiation by the Wnt pathway inhibitor ICRT3**

S5 **Rescue from toxicant-induced neural crest formation by the beta-catenin inhibitor ICRT3**

S6 **Example of the profile likelihood analysis**

S7 **Parameter confidence intervals vs. peak time**

S8 **Peak time confidence intervals**

S9 **Significance of amplitude shift**

S10 **Significance of peak time shift**

S11 **Fold change triggered by VPA for TGFβ pathway genes**

Supplementary Texts

S1 **Mathematical model of multi-state differentiation**

S2 **Analytical gradient**

S3 **Profile Likelihood**

Supplementary Table

S1 **Table of Wnt targets**

Antibody (α)	Host	Supplier	Order number	Dilution	Marker/usage
ZO1	Mouse IgG1	Invitrogen	339100	1:400	Rosette visualisation
GM130	Rabbit	Abcam	ab52649	1:400	Rosette visualisation
ISL1	Goat	Abcam	Ab109517	1:200	Neural crest
p75	Mouse IgG1	Advanced targeting systems	AB-N07	1:200	Neural crest
SOX10	Goat	Santa Cruz	sc-17342	1:500	Neural crest

Supplementary figure S1: Primary antibodies that were used for the study.

A

Primer	Marker for	Tested at	Forward seq	Reverse seq	Efficiency
NANOG	UKN1 diff.	DoD6	GGTGAAGACCTGGTTCCAGAAC	CATCCCTGGTGGTAGGAAGAGTAAAG	1.99
POU5F1B	UKN1 diff.	DoD6	GCAAAGCAGAAACCCTCGTGC	ACACTCGGACCACATCCTTCTCG	2.12
PAX6	UKN1 diff.	DoD6	CCGCCTATGCCCAGCTTCAC	AAGTGGTGCCCGAGGTGCCC	2.05
OTX2	UKN1 diff.	DoD6	GTTCAGAGTCCTTGGTGGGT	CCCTCACTCGCCACATCTAC	2.22
MSX1	Neural crest	DoD6	GGATCAGACTTCGGAGAGTGAACT	GCCTTCCCTTTAACCCTCACA	1,96
TFAP2B	Neural crest	DoD6	GGGGAGATCTTTGCGAGAAAGG	CTGTGTGCTGCCGGTTCAAATA	1.98
SNAI2	Neural crest	DoD6	CGCGCTCCTTCCTGGTCAAG	CATTGGGTAGCTGCTGGGCGTGG	2.04
PAX3	Neural crest	DoD6	GACTGGCTCCATACGTCCTGGTGC	CGGCTGATGGAACTCACTGACGG	2.08
GAD1	Wnt	DoD3	TTC TCT TCC AGG CTG TTG GT	CAA TAC CAC TAA CCT GCG CC	2.09
SP5	Wnt	DoD3	GGA CTT TGC GCA GTA CCA GAG	TGC GAC GTC TTC CCG TAC ACC	2.04
DACT	Wnt	DoD3	TGAGCTGAGTGATGGGGCTTCAGG	CTGAGGCCTGGTCTTCACAGTGGC	2,14
SIX3	Wnt	DoD3	CAA GAA CAG GCT CCA GCA C	GTG GAC GGC GAC TCT GC	2.10
RPL13A	Reference		CCTGGAGGAGAAGAGGAAAGAGA	TTGAGGACCTCTGTGTATTTGTCAA	2.01
TBP	Reference		GGGCACCACTCCACTGTATC	GCAGCAAACCGCTTGGGATTATATTCG	2.02
DAZL	Model fit	Time course	TGATCCAGGAGCTGAAGTTGTGCCAA	GCCCGACTTCTTCTAAAGTGATGCAC	2.01
BMP5	Model fit	Time course	ATCTCGGACGACTCCTCTGAC	GCTGTCACTGCCTCTCCATGA	1.97
SOX9	Model fit	Time course	AGGAAGCTCGCGGACCAGTA	CTGCCCGTTCTTCACCGACT	1.99
POU4F1	Model fit	Time course	CGG CTT GAA AGG ATG GCT CTT	CCC TGA GCA CAA GTA CCC GTC	2,07
NPY	Model fit	Time course	GCGTACCCCTCCAAGCCGGACAAC	CAGGGTCTTCAAGCCGAGTTCTGG	1.95
OLFM3	Model fit	Time course	GGCGGTGCATTTGCACAGTTGTTG	GCCGAAATTTTGCCTTCAGCCCTT	1.92
PIPOX	Model fit	Time course	GGAAGCTCCCATGGACAAAGCCGG	GCCTCGACAGATTGGCCTGGATTG	2.05

B

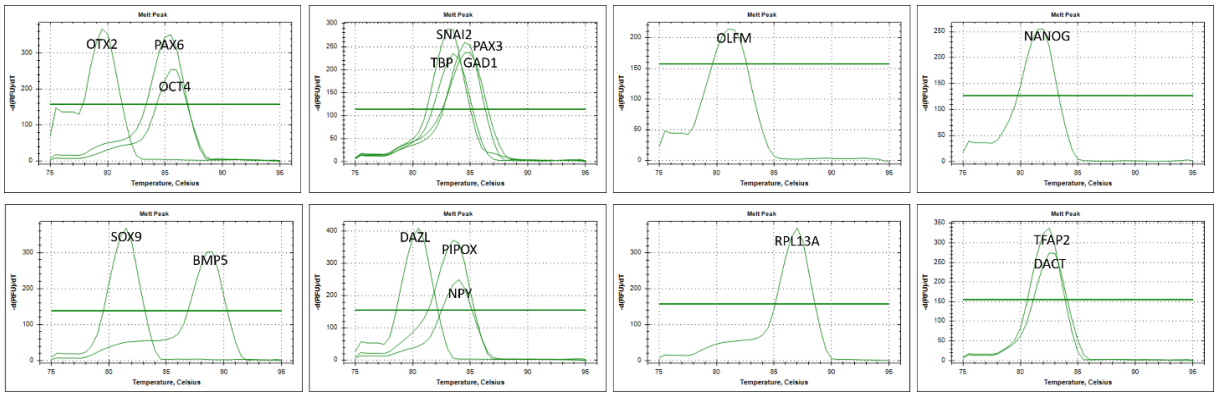

C

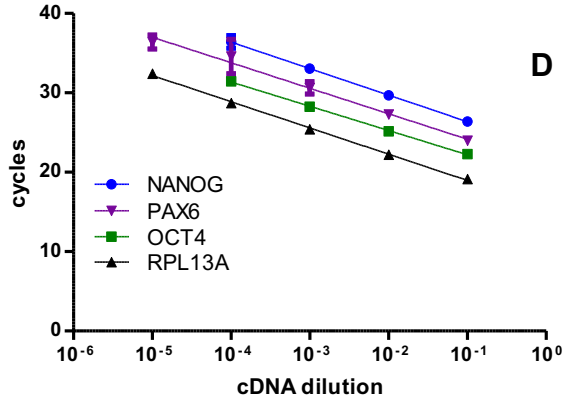

D

	NANOG	OCT4	RPL13A	PAX6
1/Slope	-0.299	-0.327	-0.303	-0.311
Efficiency	1.99	2.124	2.007	2.047
Efficiency in %	99	112	101	105
R^2	0.990	0.998	0.998	0.961

Supplementary figure S2: Primer background information.
(A) PCR Primers that were used for the study. (B) Melting curves of the PCR products. The x-axis always indiactes the temperature range from 75°C to 96°C. Notably. qPCR products were additionally analysed on their correct lenght by gel electrophoresis. Occurence of other products was excluded. (C) Standard dilution curves for major primers used for this study. (D) Primer efficiency was calculated based on the slope of standard curves.

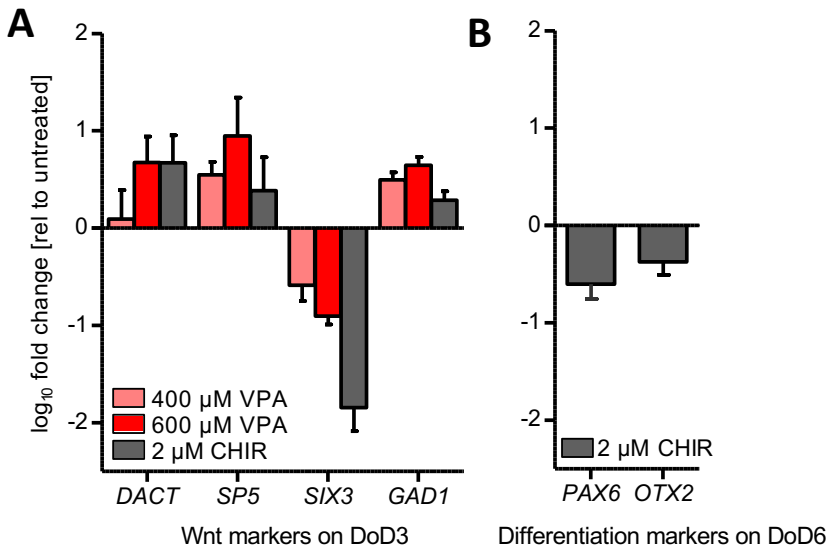

Supplementary figure S3: Wnt signaling and its consequences in the STOP-tox(UKN) assay. (A) Cells were differentiated until DoD3 using the standard STOP-tox(UKN) assay protocol (= untreated controls), or they were exposed during the differentiation to valproic acid (VPA) or the Wnt activator CHIR. Then, cells were lysed, the mRNA was isolated, and the expression of the Wnt marker genes DACT, SP5, SIX3 and GAD1 was investigated (reverse transcription real-time PCR). Data are means ± SD from three experiments. (B) Cells were differentiated as in A, but until DoD6. They were left otherwise untreated (control) or exposed to CHIR from DoD0-DoD6. Then, gene expression of the standard STOP-tox(UKN) assay endpoints PAX6 and OTX2 was measured by PCR. Data (means ± SD, n = 3) is depicted relative to the untreated control. The data confirm previous findings (8) that Wnt activation affects the assay outcome.

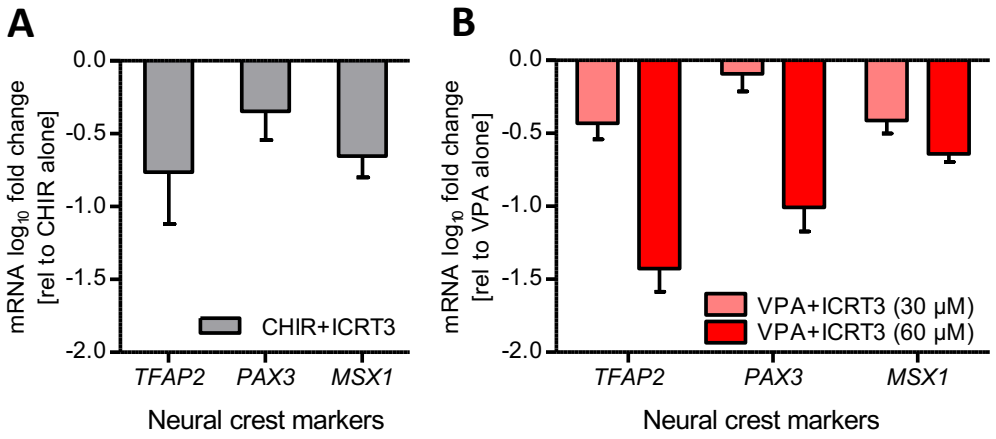

Supplementary figure S4: Attenuation of neural crest differentiation by the Wnt pathway inhibitor ICRT3. Cells were differentiated until DoD6 using the standard STOP-tox(UKN) assay protocol, modified by the addition of CHIR (2 µM) or VPA (400 µM), two toxicants shifting the differentiation from the neuroepithelial lineage towards neural crest (8,9). On DoD6, the expression of marker genes was analyzed by PCR. (A) Cells were treated with CHIR alone, or the beta-catenin inhibitor ICRT3 (60µM) was added in addition from DoD2-6. The expression of the neural crest marker genes TFAP2, PAX3 and MSX1 was investigated, and data are indicated as CHIR+ICRT3 vs CHIR alone. Negative numbers on the abscissa indicate a relative downregulation (= attenuation of the CHIR effect) by ICRT3. (B) Cells were treated with VPA alone, or the beta-catenin inhibitor ICRT3 (30 µM and 60µM) was added in addition from DoD2-6. The expression of the neural crest marker genes TFAP2, PAX3 and MSX1 was investigated, and data are indicated as VPA+ICRT3 vs VPA alone. Negative numbers on the abscissa indicate a relative downregulation (= attenuation of the VPA effect) by ICRT3. All data are means ± SD, n=3.

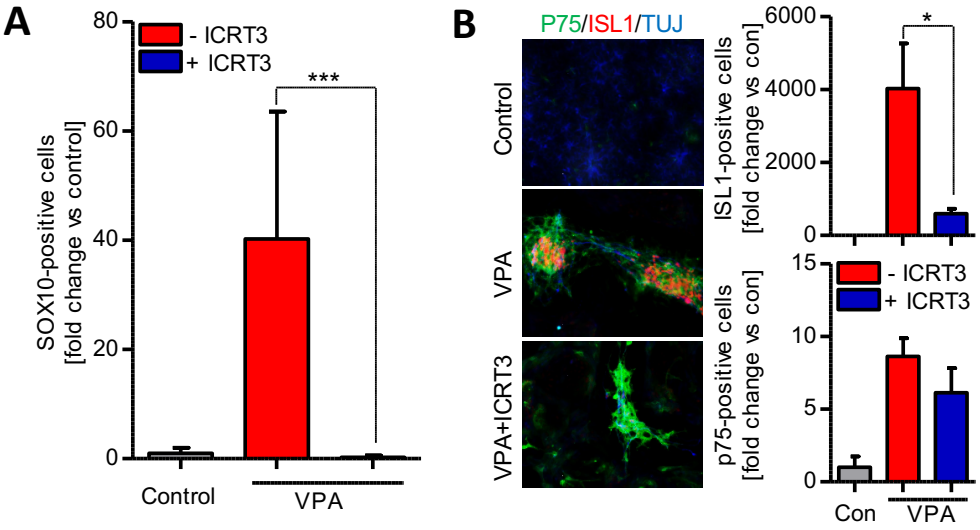

Supplementary figure S5: Rescue from toxicant-induced neural crest formation by the beta-catenin inhibitor ICRT3. (A) Pluripotent stem cells were differentiated until DoD6, and exposed to solvent or valproic acid (VPA, 600 µM) from DoD0-DoD6. They were co-treated or not with ICRT3 (beta-catenin inhibitor; 60 µM) from DoD2-DoD6. Then, SOX10 protein was immunostained, and the number of positive cells was quantified (SOX10 positive pixels were counted automatically and they were normalized to the nuclear area, as identified by H-33342 staining). Data are means ± SD; n=3. The untreated control (Con; differentiation without toxicants or inhibitors) is used as reference to calculate fold-changes of treated cells. (B) Pluripotent stem cells were differentiated until DoD15, and exposed to valproic acid (VPA, 600 µM) from DoD0-DoD6. They were co-treated with ICRT3 from DoD2-DoD6. On DoD15, cells were fixed and immunostained for ISL1 and p75 (the low affinity nerve growth factor receptor NGFR, aliases: TNFRSF16, CD271, p75NTR). The number of positive cells was quantified as in A in 7-16 wells. Data are means ± SD. Data is shown relative to untreated control (Con).

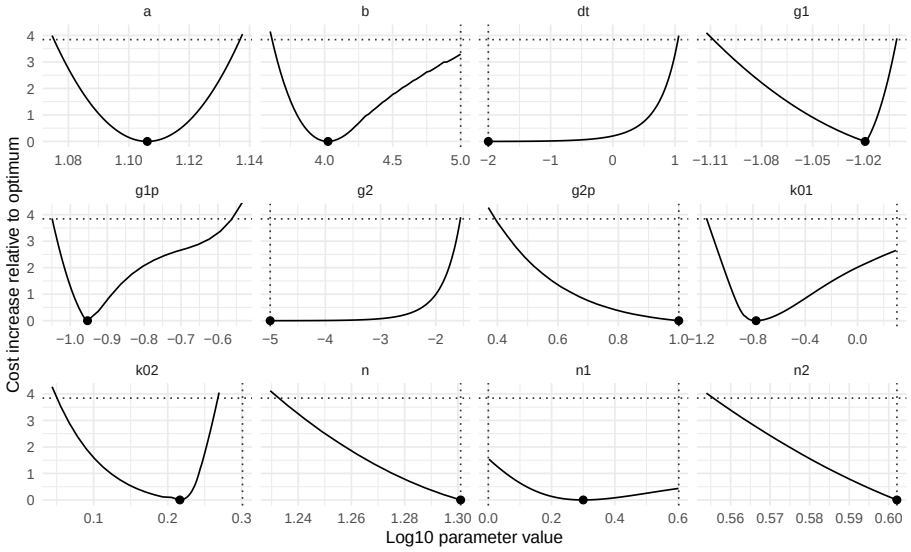

Supplementary Figure S6: Example of the profile likelihood analysis for the gene POU4F1 using the L-BFGS-B optimization algorithm. For each parameter, the cost difference to the minimal cost is plotted against the parameter value.

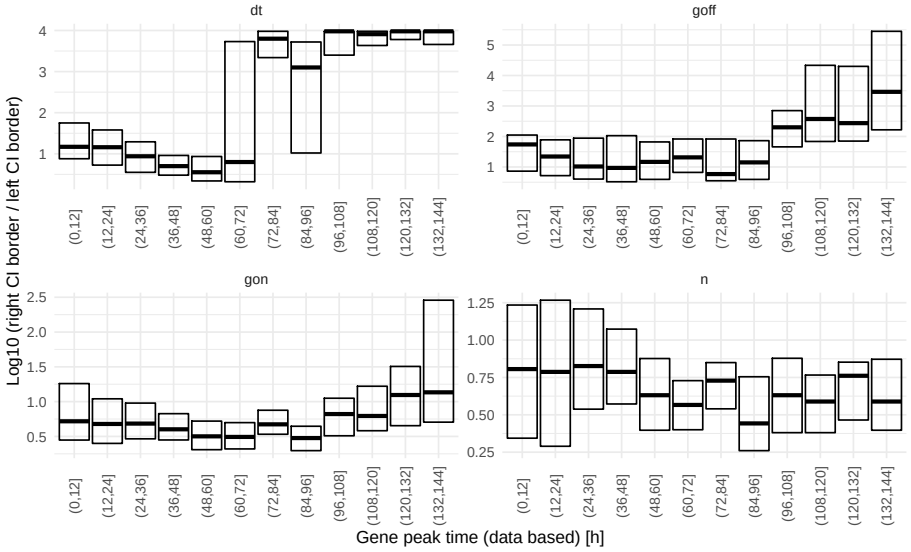

Supplementary Figure S7: Box plots showing the distribution of the parameter confidence intervals for the parameters g_{on}, g_{off}, n and dt. Genes peaking later than 0 h or earlier than 144 h were binned by their peak time into 12 hour intervals based on the data (interpolated using loess with span 0.8 to a resolution of 0.1 h) and the 25%, 50% and 75% quantiles of the Log10 ratio of the upper and lower confidence interval boundary were computed in each bin. Boxes indicate the interquartile distribution, horizontal bars the median.

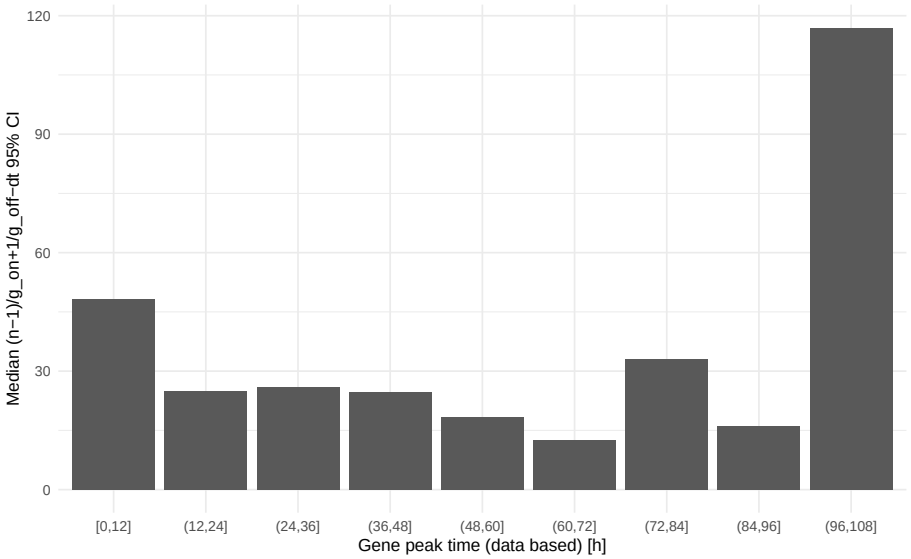

Supplementary Figure S8: Median confidence interval for the peak time approximated by $(n-1)/g_{\text{on}} + 1/g_{\text{off}} - dt$ according to Eq. (11). Genes were binned into 12 hour intervals as in Fig. S7 and the median confidence interval for the peak time as a function of the parameters g_{on}, g_{off}, n and dt was computed in each bin. Bins for genes peaking later than 108 h were excluded and only genes peaking later than 0 h were included.

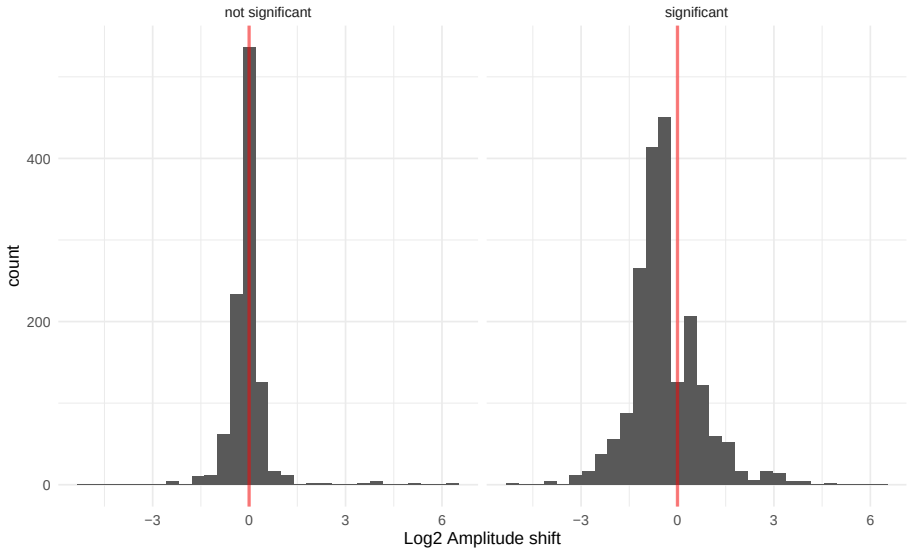

Supplementary Figure S9: Distribution of genes with respect to the amplitude shift triggered by 0.6 mM VPA compared to the untreated differentiation for genes with and without significant shift. Only genes with an amplitude shift confidence interval excluding zero are considered significant.

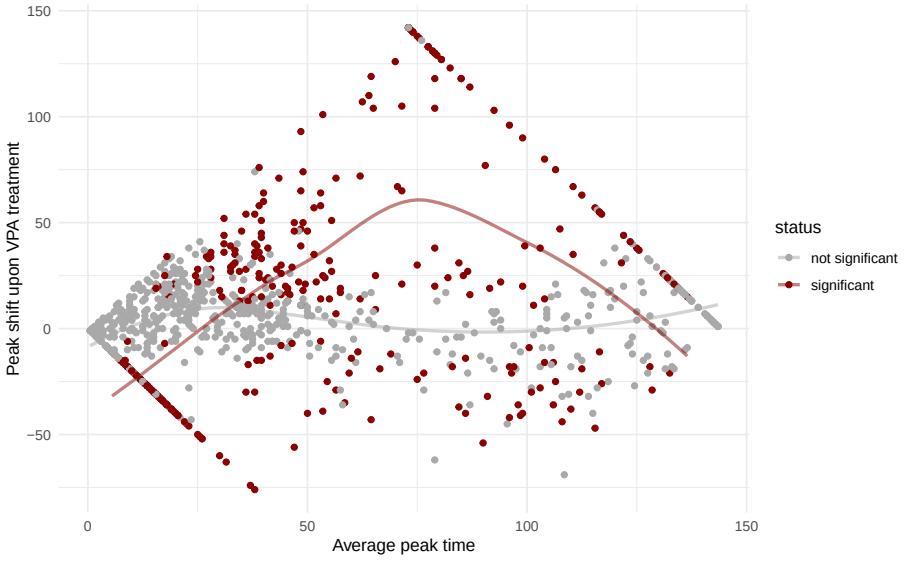

Supplementary Figure S10: MA-plot for the change in peak time triggered by 0.6 mM VPA compared to the untreated differentiation. For each gene that peaks later than 0 h and earlier than 144 h in the fit to the untreated data, the change in peak time is plotted against the mean of the peak time in the treated and untreated conditions. Genes with a peak time shift confidence interval excluding zero are marked in red. Lines indicate a loess interpolation with span 0.75.

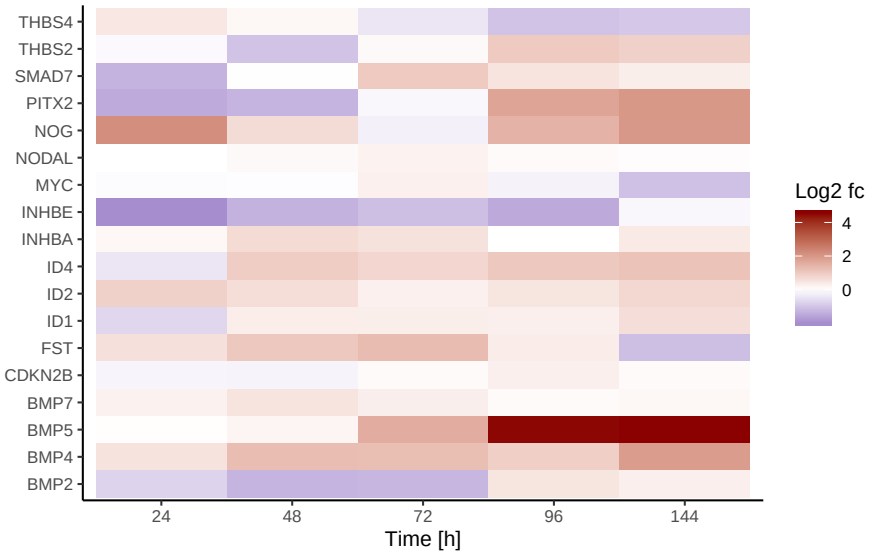

Supplementary Figure S11: The fold change between cells treated with 0.6 mM VPA and untreated cells is shown as a heatmap for TGFβ pathway genes at the indicated time points.

Supplementary Text S1 Mathematical model of multi-state differentiation

The multi-state kinetic model can be described by the Bateman equation (Bateman, 1910) originally formulated for radioactive decay chains. We will use the special case where an intermediate state n is preceded by $n-1$ states with transition rate g_{on} and decays with rate g_{off}. In this case the differential equation is

$$\begin{aligned}
\frac{\partial p_0}{\partial t} &= -g_{\mathrm{on}} p_0 && (1)\\
\frac{\partial p_1}{\partial t} &= g_{\mathrm{on}} p_0 - g_{\mathrm{on}} p_1 && (2)\\
\ldots &\quad \ldots && (3)\\
\frac{\partial p_n}{\partial t} &= g_{\mathrm{on}} p_{n-1} - g_{\mathrm{off}} p_n && (4)
\end{aligned}$$

For $n \geq 1$ and $p_0(0) = 1$ we have the solution (Ritter et al., 2003)

$$p_n = e^{-g_{\mathrm{off}} t} \left(\frac{g_{\mathrm{on}}}{g_{\mathrm{on}} - g_{\mathrm{off}}} \right)^n \left(1 - \frac{\Gamma(n, t(g_{\mathrm{on}} - g_{\mathrm{off}}))}{\Gamma(n)} \right), \qquad (5)$$

with $\Gamma(n)$ the gamma function and $\Gamma(n,x)$ the upper incomplete gamma function. The upper incomplete gamma function can be replaced by the lower incomplete gamma function $\gamma(n,x)$ according to

$$1 - \frac{\Gamma(n,x)}{\Gamma(n)} = \frac{\gamma(n,x)}{\Gamma(n)} = \frac{n^{-1} x^n \mathrm{M}(n, 1+n, -x)}{\Gamma(n)}. \qquad (6)$$

The last step used a relationship between the gamma function and the confluent hypergeometric function found in Abramowitz and Stegun (1964) as equation 6.5.12. Plugging (6) into (5) , we obtain

$$p_n = \frac{e^{-g_{\mathrm{off}} t} g_{\mathrm{on}}^n t^n \mathrm{M}(n, 1+n, -(g_{\mathrm{on}} - g_{\mathrm{off}})t)}{\Gamma(n+1)}, \qquad (7)$$

where $n\Gamma(n) = \Gamma(n+1)$ has been used. For $g_{\mathrm{off}} \gg_{\mathrm{on}}$ the confluent hypergeometric function $\mathrm{M}(n, 1+n, -(g_{\mathrm{on}} - g_{\mathrm{off}})t)$ becomes too large for standard machine size numbers. Using Kummer's transformation $\mathrm{M}(a,b,x) = e^x \mathrm{M}(b-a, b, -x)$ (Abramowitz and Stegun (1964), 13.1.14), we can avoid this problem by taking

$$p_n = \frac{e^{-g_{\mathrm{on}} t} g_{\mathrm{on}}^n t^n M(n, 1+n, (g_{\mathrm{on}} - g_{\mathrm{off}})t)}{\Gamma(n+1)} \qquad (8)$$

instead of (7) for $g_{\mathrm{off}} > g_{\mathrm{on}}$. The confluent hypergeometric function $\mathrm{M}(a,b,x)$ is implemented as hyperg_1F1(a,b,x) in the GNU scientific library which is available

through the R package `gsl`. As every term in our solution is defined for real positive n, we do not need to restrict ourselves to integer number of steps.

If g_{off} is large, the rather complicated solution for p_n can be formulated in terms of p_{n-1}, which helps to find the time where the maximum occurs. More precisely, Ritter et al. (2003) show that

$$\lim_{g_{\text{off}} \to \infty} g_{\text{off}}\, p_n = g_{\text{on}}\, p_{n-1}. \tag{9}$$

With the equal transition rate solution for the Bateman equations,

$$p_{n-1} = \frac{1}{(n-1)!} e^{-g_{\text{on}} t} (g_{\text{on}} t)^{n-1}, \tag{10}$$

we can approximate the time of the maximum for p_n by the maximum of p_{n-1}, $t = (n-1)/g_{\text{on}}$. If p_n is linearly extrapolated around $t_{max} = (n-1)/g_{\text{on}}$, the equation $g_{\text{on}} p_{n-1}(t_{max}) = g_{\text{off}} p_n(t_{max} + \Delta t)$ is satisfied for $\Delta t = 1/g_{\text{off}}$ (The linear expansion of p_{n-1} lacks the first order term because its evaluated at the maximum). It follows that the approximation of the maximum of p_n by the maximum of p_{n-1} is good for $\frac{n-1}{g_{\text{on}}} \gg \frac{1}{g_{\text{off}}}$. A better approximation that is valid for large g_{off} is

$$t_{max} = \frac{n-1}{g_{\text{on}}} + \frac{1}{g_{\text{off}}}. \tag{11}$$

Supplementary Text S2 Analytical gradient

To improve optimizer performance at parameter values where the cost function is shallow, we implemented an analytical gradient for the cost function. We list the derivatives of (8) with respect to n, t, g_{on} and g_{off}.

$$\begin{aligned}
&\frac{d}{dn} p_n = \frac{1}{n\Gamma(n)} \exp\left(-g_{\text{off}} t\right) \times \\
&\left(1 - \frac{g_{\text{off}}}{g_{\text{on}}}\right)^{-n} \Big(-((g_{\text{on}} - g_{\text{off}})t)^n \text{HyperG}_{2\text{F}2}((n,n),(1+n,1+n),(-g_{\text{on}} + g_{\text{off}})t) \\
&(\Gamma(1+n) - n\Gamma(n,(g_{\text{on}} - g_{\text{off}})t))(1 + \bar{\gamma} n - n H_n + n \log(g_{\text{on}} t)) \Big),
\end{aligned}$$

where $\bar{\gamma}$ is the Euler-Mascheroni constant, H_n is the n-th harmonic number and $\text{HyperG}_{2\text{F}2}$ is the generalized hypergeometric function 2F2. Since we did not find an R-implementation of $\text{HyperG}_{2\text{F}2}$ we used the integral representation Eq. (4.8.3.11) in Slater (1966):

$${}_2F_2((a,d),(b,c),x) = \frac{\Gamma(a)}{\Gamma(b) - \Gamma(a)} \int_0^1 {}_1F_1(d,c,xt)\mathrm{d}t.$$

For t:

$$\frac{d}{dt}p_n = \frac{1}{t\Gamma(n)}\exp\left(-g_{\text{on}}t\right)g_{\text{on}}^n(g_{\text{on}}-g_{\text{off}})^{-n}\times$$
$$(((g_{\text{on}}-g_{\text{off}})t)^n - \exp\left((g_{\text{on}}-g_{\text{off}})t\right)g_{\text{off}}t(\Gamma(n)-\Gamma(n,(g_{\text{on}}-g_{\text{off}})t)))\,.$$

For g_{on}:

$$\frac{d}{dg_{\text{on}}}p_n = \frac{1}{\Gamma(n)}\exp\left(-g_{\text{on}}t\right)g_{\text{on}}^{n-1}(g_{\text{on}}-g_{\text{off}})^{-n-1}\times$$
$$(g_{\text{on}}((g_{\text{on}}-g_{\text{off}})t)^n - \exp\left((g_{\text{on}}-g_{\text{off}})t\right)g_{\text{off}}n(\Gamma(n)-\Gamma(n,(g_{\text{on}}-g_{\text{off}})t)))\,.$$

For g_{off}:

$$\frac{d}{dg_{\text{on}}}p_n = \frac{1}{\Gamma(n)}\exp\left(-g_{\text{on}}t\right)g_{\text{on}}^{n}(g_{\text{on}}-g_{\text{off}})^{-n-1}\times$$
$$(-((g_{\text{on}}-g_{\text{off}})t)^n - \exp\left((g_{\text{on}}-g_{\text{off}})t\right)(n+(g_{\text{off}}-g_{\text{on}})t)(\Gamma(n)-\Gamma(n,(g_{\text{on}}-g_{\text{off}})t)))\,.$$

The full cost function is a sum over terms of the form

$$\frac{\left(y_i - \log_2\left(A + Bp_n(t_i, h(c_i, g_{\text{on}}, g'_{\text{on}}, k_1, n_1), h(c_i, g_{\text{off}}, g'_{\text{off}}, k_2, n_2), n)\right)\right)^2}{\sigma_i^2},$$

where t_i, c_i, y_i and σ_i are the time point, concentration, measured expression and standard deviation for one condition. Furthermore, $h(c, g, g', k, n)$ is a Hill function of the form

$$g + (g - g')\frac{c^n}{c^n + k^n}.$$

Consequently, derivatives of the cost function have to be computed using the chain rule. We exemplify this for the parameter k_1.

$$-2\frac{B\left(y_i - \log_2(A + Bp_n)\right)}{\sigma_i^2(A + Bp_n)\log(2)}\frac{d}{dg_{\text{on}}}p_n\frac{d}{dk}h(c, g_{\text{on}}, g_{\text{off}}, k_1, n_1),$$

where we ommitted the arguments of p_n for brevity. Derivatives for all other parameters can be computed in a similar fashion.

Supplementary Text S3 Profile Likelihood

To analyze parameter identifiability, we performed profile likelihood (PL) as described in Kreutz et al. (2013). First, optimal parameter sets were reoptimized using the L-BFGS-B method implemented in the optim function using parameters maxit=20000, fnscale=1e6, factr=1e2. This was done because PL results are quite

Algorithm	Parameters
LM	ftol=10^{-25}, ptol=10^{-16},gtol=10^{-15}, maxiter=$2 \cdot 10^4$
LBFGSB	fnscale=10^6, factr=10^2 maxit=$2 \cdot 10^4$

Table 1: Parameters used for optimization.

sensitive to small deviations from the optimal parameter set. A fixed step size in log space of $\frac{log10(u)-log10(l)}{200}$, where u and l are the parameter upper and lower bounds, respectively, was chosen for the PL parameter. PL parameter values where increased/decreased by the fixed step size starting from the optimal value and all other parameters where reoptimized after each step. Computation of the costs after each step increase/decrease was terminated when the cost increase exceed the 95%-quantile of the χ^2 distribution with one degree of freedom or if the parameter value exceeded the upper or lower bound. If termination occured and less than 10 steps were performed, the step size was decreased until the parameter was increased and decreased from the optimum by at least 10 steps.

We observed that the results of the PL analysis vary strongly with the parameters supplied to the optimizer function. In particular, sometimes the optimizer oscillated between two similar local optima between PL steps. Because of this we decided to compute the PL with two different optimization algorithms to reduce the influence of the details of the optimization strategy on the parameter identifiability results. We used the parameters indicated in Tab. 1 for the optimization algorithms. For each gene and parameter, we used the largest PL interval predicted by any of the two procedures. Exemplary profile likelihood plots for the gene POU4F1 are shown in Fig. S6.

When a lower cost (minimal cost improvement 0.01) than the optimal cost obtained during fitting was encountered in the PL analysis, we reran the PL analysis starting from the parameter set corresponding to the lower cost value.

Finally, the best parameter set encountered for each gene during the initial fit or during the PL analysis was adopted as final parameter set and used to generate model predictions.

References

Abramowitz, M. and Stegun, I. A. (1964). *Handbook of Mathematical Functions: With Formulas, Graphs, and Mathematical Tables*. Courier Corporation. Google-Books-ID: MtU8uP7XMvoC.

Bateman, H. (1910). The solution of a system of differential equations occurring in the theory of radioactive transformations. In *Proc. Cambridge Philos. Soc*, volume 15, pages 423–427.

Kreutz, C., Raue, A., Kaschek, D., and Timmer, J. (2013). Profile likelihood in systems biology. *The FEBS Journal*, 280(11):2564–2571.

Ritter, G., Wilson, R., Pompei, F., and Burmistrov, D. (2003). The multistage model of cancer development: some implications. *Toxicology and Industrial Health*, 19(7-10):125–145.

Slater, L. J. (1966). *Generalized Hypergeometric Functions*. Cambridge University Press. Google-Books-ID: Hq0NAQAAIAAJ.

Supplementary Table S1 Wnt targets

gene	symbol	z_value_wnt_induction
ENSG00000138083	SIX3	-16.1516627014814
ENSG00000134595	SOX3	-10.315654290238
ENSG00000163666	HESX1	-8.54100694986801
ENSG00000181274	FRAT2	-8.02413276419602
ENSG00000126010	GRPR	-7.05541558644029
ENSG00000170955	PRKCDBP	-6.98243425681697
ENSG00000048545	GUCA1A	-6.25124030674909
ENSG00000147257	GPC3	-6.19639113716754
ENSG00000118513	MYB	-6.0877600645586
ENSG00000118523	CTGF	-5.88648163315426
ENSG00000113763	UNC5A	-5.88632390438663
ENSG00000008311	AASS	-5.71180581054374
ENSG00000178573	MAF	-5.5640485810582
ENSG00000125378	BMP4	-5.44667351333135
ENSG00000184302	SIX6	-5.37124241645972
ENSG00000134207	SYT6	-5.33975536154076
ENSG00000176788	BASP1	-5.28342300181845
ENSG00000169764	UGP2	-5.2762105139029
ENSG00000163251	FZD5	-5.2510067051812
ENSG00000111913	FAM65B	-5.14287478722049
ENSG00000050344	NFE2L3	-5.07012501898418
ENSG00000141736	ERBB2	-5.05526267230371
ENSG00000249992	TMEM158	-4.94758118436699
ENSG00000163694	RBM47	-4.81438303928001
ENSG00000076716	GPC4	-4.67079948358355
ENSG00000111752	PHC1	-4.64599069647958
ENSG00000162496	DHRS3	-4.58392112519483
ENSG00000147601	TERF1	-4.46565814725689
ENSG00000128610	FEZF1	-4.46534454951203
ENSG00000154553	PDLIM3	-4.42266413987513
ENSG00000142871	CYR61	-4.40940113486154
ENSG00000141682	PMAIP1	-4.28944741034966
ENSG00000179046	TRIML2	-4.28913581208809
ENSG00000165029	ABCA1	-4.25418302886945
ENSG00000140511	HAPLN3	-4.22415090943536
ENSG00000118407	FILIP1	-4.19574953779071
ENSG00000106829	TLE4	-4.17213934066303
ENSG00000118946	PCDH17	-4.16753298419809
ENSG00000135525	MAP7	-4.15601387750254
ENSG00000077274	CAPN6	-4.01782484192113
ENSG00000106538	RARRES2	-4.00565621277993
ENSG00000102119	EMD	-3.97242570442417
ENSG00000158321	AUTS2	-3.96290679687107
ENSG00000154556	SORBS2	-3.96074103559565
ENSG00000171608	PIK3CD	-3.95502181792838
ENSG00000073712	FERMT2	-3.92033220959351
ENSG00000134324	LPIN1	-3.88564019596438
ENSG00000156475	PPP2R2B	-3.8585950831058
ENSG00000130751	NPAS1	-3.85682257182812

ENSG00000171246	NPTX1	-3.83797349974686
ENSG00000035403	VCL	-3.72642899522194
ENSG00000185885	IFITM1	-3.71290054866807
ENSG00000146411	SLC2A12	-3.70055133364338
ENSG00000140545	MFGE8	-3.69729614186889
ENSG00000150687	PRSS23	-3.65305448075273
ENSG00000100605	ITPK1	-3.65043054422015
ENSG00000181885	CLDN7	-3.60015782261828
ENSG00000116774	OLFML3	-3.58884789978521
ENSG00000124839	RAB17	-3.5812186615456
ENSG00000147676	MAL2	-3.57864737091821
ENSG00000129654	FOXJ1	-3.55528028946606
ENSG00000129116	PALLD	-3.53943467309711
ENSG00000135248	FAM71F1	-3.50511379837745
ENSG00000074410	CA12	3.52258646667265
ENSG00000136842	TMOD1	3.52581091010396
ENSG00000151692	RNF144A	3.57292505103783
ENSG00000165495	PKNOX2	3.61128756037628
ENSG00000171100	MTM1	3.64756243261209
ENSG00000115738	ID2	3.65826081117459
ENSG00000166974	MAPRE2	3.70182338104162
ENSG00000116871	MAP7D1	3.72334617184995
ENSG00000170549	IRX1	3.73257051343592
ENSG00000169306	IL1RAPL1	3.75386905218784
ENSG00000018625	ATP1A2	3.80897043298757
ENSG00000199102	MIR302C	3.81760280829055
ENSG00000079739	PGM1	3.86540684126316
ENSG00000140455	USP3	3.90725181354598
ENSG00000104267	CA2	3.92493716790639
ENSG00000158966	CACHD1	3.9842574891187
ENSG00000146426	TIAM2	4.00761925460455
ENSG00000117394	SLC2A1	4.05107269727051
ENSG00000177508	IRX3	4.0574188032457
ENSG00000188257	PLA2G2A	4.14547505306511
ENSG00000100314	CABP7	4.17434697846671
ENSG00000165617	DACT1	4.25811170096308
ENSG00000157570	TSPAN18	4.26563756457701
ENSG00000138764	CCNG2	4.2862632491678
ENSG00000079215	SLC1A3	4.33470659238981
ENSG00000103710	RASL12	4.43018307882895
ENSG00000113916	BCL6	4.70189991851954
ENSG00000022267	FHL1	4.728215674998
ENSG00000126822	PLEKHG3	4.78526555497771
ENSG00000170561	IRX2	4.81391170337348
ENSG00000134569	LRP4	4.8704608689237
ENSG00000110675	ELMOD1	4.88908144562804
ENSG00000137193	PIM1	4.99770222860548
ENSG00000071575	TRIB2	5.00432385531391
ENSG00000101384	JAG1	5.01362883735314
ENSG00000090776	EFNB1	5.02633193962582
ENSG00000169071	ROR2	5.4560709192239
ENSG00000176842	IRX5	5.58956840068819
ENSG00000127863	TNFRSF19	5.65567356152472

ENSG00000134363	FST	5.78598409986394
ENSG00000262655	SPON1	5.81420604714459
ENSG00000115290	GRB14	6.49415569572562
ENSG00000100767	PAPLN	6.57383963292784
ENSG00000175352	NRIP3	6.73567882345321
ENSG00000137267	TUBB2A	6.77033643297005
ENSG00000168646	AXIN2	6.77759262595111
ENSG00000143878	RHOB	7.01401690969806
ENSG00000136205	TNS3	7.07831021322305
ENSG00000174498	IGDCC3	7.23243121251923
ENSG00000173320	STOX2	7.27395256432328
ENSG00000197587	DMBX1	7.51839630501491
ENSG00000184144	CNTN2	8.35277558864278
ENSG00000171724	VAT1L	9.07115336213258
ENSG00000128683	GAD1	9.13522059983478
ENSG00000125492	BARHL1	9.27819453247737
ENSG00000204335	SP5	11.8446495530989